Thermoelectric properties of layered perovskite-type $(Sr_{1-x}Ca_x)_3(Ti_{1-y}Nb_y)_2O_7$

Kyu Hyoung Lee
CREST-Japan Science and Technology Agency, 4-1-8 Honcho, Kawaguchi 332-0012, Japan

Sung Wng Kim
Frontier Collaborative Research Center, Tokyo Institute of Technology, 4259 Nagatsuta, Midori, Yokohama 226-8503, Japan

Hiromichi Ohta and Kunihito Koumoto[a)]
Graduate School of Engineering, Nagoya University, Nagoya 464-8603, Japan
and CREST-Japan Science and Technology Agency, 4-1-8 Honcho, Kawaguchi 332-0012, Japan

(Received 25 October 2006; accepted 11 February 2007; published online 24 April 2007)

The thermoelectric properties and crystallographic features of layered perovskite-type Ca-substituted $(Sr_{1-x}Ca_x)_3(Ti_{1-y}Nb_y)_2O_7$ ($y=0-0.2$), Ruddlesden-Popper phases were investigated. The influence of crystal structure and carrier concentration on the carrier effective mass for Ti-based metal oxides based on TiO_6 octahedra and having a significant Ca substitution effect are discussed. It was found from structural analysis that the large Seebeck coefficients of Ca-substituted compounds can be attributed to the high values of carrier effective mass, which originates from the enhancement of the symmetry of the TiO_6 octahedra. Low thermal conductivities, 3.6–3.8 W m^{-1} K^{-1} at 300 K, were obtained for Ca-substituted compositions due to phonon scattering at $SrO/(SrTiO_3)_2$ interfaces of the inherent superlattice structure and to mass-defect phonon scattering between Ca ($M_{Ca}=40$) and Sr ($M_{Sr}=88$). The highest ZT value obtained was 0.15 at 1000 K, for 10 at % Ca-substituted $Sr_3(Ti_{0.95}Nb_{0.05})_2O_7$. © *2007 American Institute of Physics*. [DOI: 10.1063/1.2718280]

I. INTRODUCTION

Perovskite-type oxides form the basis for several polysomatic series. One such structural group is known as the layered perovskite-type Rudlesdden-Popper (RP) phase, with the general formula $AO(ABO_3)_n$ (n=integer).[1,2] These structures are based upon the insertion of n ABO_3 block layers of the perovskite structure between single distorted NaCl-type AO interlayers. RP phases exhibit a number of attractive properties such as superconductivity,[3] dielectric characteristic,[4] magnetoresistance,[5] ionic conductivity,[6] oxygen permeation,[7] and catalysis,[8] owing to their unique structural characteristics, which include the presence of perovskite block layers.

RP phases can be regarded as a superlattice that has an intrinsic ability to exhibit a low lattice thermal conductivity (κ_{lat}), due to the enhancement of phonon scattering at the numerous internal interfaces in these $AO/(ABO_3)_n$ compounds.[9] Because low thermal conductivity (κ) is a very attractive property for thermoelectric (TE) applications, we have investigated the suitability of RP phases as TE materials by using Nb-doped $SrO(SrTiO_3)_n$ ($n=1,2$) bulk polycrystalline samples.[10] Compared with the cubic perovskite-type Nb-doped $SrTiO_3$, κ_{lat} was substantially reduced by the enhancement of phonon scattering at $SrO/(SrTiO_3)_n$ interfaces, and the maximum dimensionless figures of merit ZT were fairly large in these TE oxide materials, (0.09 – 0.14 at 1000 K). However, these ZT values are still low compared with those of cubic perovskite-type Nb-doped $SrTiO_3$ ($ZT=0.37$ at 1000 K),[11,12] which exhibits the highest TE performance among the n-type TE oxides. One reason for the low ZT values of polycrystalline RP compounds has been recognized to be their relatively low electrical conductivity (σ) by random distribution of insulating SrO layers. Such a low σ is a secondary consideration in the sense that high σ could be attained by the synthesis of textured ceramics in which the crystal axis is oriented in one direction or epitaxial thin films. The central issue for the low TE performance of RP phases is the low Seebeck coefficient (S), which originates from the small carrier effective mass (m^*) and is a property intrinsic to the material rather than to the polycrystalline properties.

In a previous article,[10] we investigated the effect of the shape of the TiO_6 octahedra on the TE properties of RP phases. RP phases have deformed TiO_6 octahedra, a feature which leads to the crystal field splitting of Ti $3d-t_{2g}$ orbitals (splitting of degeneracy), and this characteristic feature of the RP phase results in small m^* (small S) values. In order to maximize S via modification of the symmetry the TiO_6 octahedra, Ba and Ca substitution at the Sr site was considered. However, it was very difficult to obtain a single phase in Ba-substituted compositions due to the low phase formation energy of many other Ba-Nb-O compounds. Thus, in the present study, the relationships between the transport parameters, including S, m^*, and carrier concentration (n_c), and the crystallographic parameters, including the Ti-O bond length and the O-Ti-O bond angle, of $(Sr_{1-x}Ca_x)_3(Ti_{1-y}Nb_y)_2O_7$ (x

[a)]Author to whom correspondence should be addressed; electronic mail: koumoto@apchem.nagoya-u.ac.jp

=0, 0.1, y=0.05–0.2) RP phases was investigated in order to clarify the origin of TE properties in Ti-based metal oxides containing TiO_6 octahedra.

II. EXPERIMENT

High-purity (>99.9%) $SrCO_3$, $CaCO_3$, TiO_2, and Nb_2O_5 powders were processed by the solid-state reaction method to form compounds in the $(Sr_{1-x}Ca_x)_3(Ti_{1-y}Nb_y)_2O_7$ (x =0, 0.1, y=0.05–0.2) system. Starting powders were mixed for 1 h in a planetary ball mill and calcined for 12 h at 1200 °C in air. In order to form the RP phases and generate the electron carriers through the reduction of Ti^{4+} to Ti^{3+} by doping of Nb^{5+}, the powder was heated at 1400 – 1475 °C for 1–2 h in a carbon crucible under an Ar atmosphere. Then, after ball milling again for 1 h, highly dense polycrystalline ceramic samples were fabricated by conventional hot pressing (36 MPa and 1400 – 1475 °C for 1 h in an Ar flow). Structural parameters obtained from the x-ray diffraction data were refined by the Rietveld method by use of the RIETAN-2000 program.[13] The σ and S values were measured from 300 to 1000 K by a conventional dc 4-probe method and a steady-state method, respectively, in flowing Ar. The Hall mobility (μ_{Hall}) and n_c values were measured with the van der Pauw configuration under vacuum. The κ values were calculated by separate measurements with differential scanning calorimetry for heat capacity and a laser-flash method for thermal diffusivity under vacuum.

III. RESULTS AND DISCUSSION

The $Sr_3Ti_2O_7$ single phase was produced in the compounds of $y \leq 0.2$ and x=0 in the $(Sr_{1-x}Ca_x)_3(Ti_{1-y}Nb_y)_2O_7$ (x=0, 0.1, y=0.05–0.2) system, while $Sr_4Nb_2O_9$ was produced as a secondary phase for the compounds with y=0.2 and Ca substitution (x=0.1). This result can be explained in terms of a tolerance factor[14] that is well known as a parameter of perovskite-type structural stability,

$$\text{tolerance factor} = \frac{(r_A + r_O)}{\sqrt{2}(r_B + r_O)},$$

where r_A, r_B , and r_O are the average ionic radii of the A-site cation, B-site cation, and oxygen ion, respectively. When this factor is close to 1, the perovskite-type structure becomes more stable. From the fact that the tolerance factor of $SrTiO_3$ is about 1.0 and is decreased by doping of Nb^{5+} ion (r =64 p.m., coordination number =6) at Ti^{4+} sites (r =60.5 p.m., coordination number =6), as well as by substituting Ca^{2+} ions (r=134 p.m., coordination number =12) at Sr^{2+} sites (r=144 p.m., coordination number =12),[15] it can be rationalized that the solubility limit of Nb^{5+} ions at Ti sites decreases in the Ca-substituted compositions.

The structural analysis was conducted by use of a Rietveld refinement based on the space group $I4/mmm$ (no. 139). The reliability factor R_{wp} was ~10% in all compounds, and the crystallographic data obtained at room temperature are shown in Fig. 1. It was found that the lattice parameters (a,c) and volume (V) increased gradually with an increase in Nb content and decreased with Ca substitution. These trends of structural change can be attributed to the fact that the

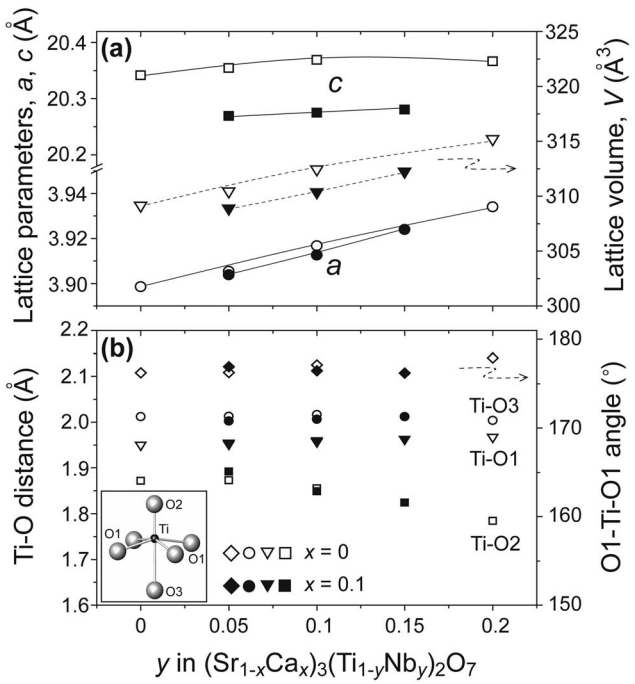

FIG. 1. Variation of crystallographic parameters for $(Sr_{1-x}Ca_x)_3(Ti_{1-y}Nb_y)_2O_7$ (x=0, 0.1, y=0.05–0.2) with Ca and Nb content (a) lattice parameters and volume and (b) Ti-O distance and O1-Ti-O1 angle. The shape of the TiO_6 octahedron is shown in the inset.

radius of the Ca^{2+} ion is smaller than that of the Sr^{2+} ion, the Nb^{5+} ion is slightly larger than that of the Ti^{4+} ion, and larger Ti^{3+} ions (r=67 p.m., coordination number =6) are created by Nb doping. The inset of Fig. 1(b) shows the schematic structure of TiO_6 octahedra in perovskite layers of $Sr_3Ti_2O_7$. There are three different Ti-O bonds (Ti-O1, Ti-O2, and Ti-O3), and the Ti ion is situated slightly above the O1 ions along the c-axis. As a result, the Ti-O1 layers are not flat but are slightly corrugated, and the TiO_6 octahedra in $Sr_3Ti_2O_7$ are not of the regular type. The lengths of the three Ti-O bonds and the angle of the O1-Ti-O1 bond were calculated in order to investigate the shapes of the TiO_6 octahedra, and the data obtained are presented in Fig. 1(b). For all compositions, the Ti-O1 and Ti-O3 bond lengths were almost the same, while the Ti-O2 bond length gradually decreased, and thus the differences in bond length become larger with increasing Nb content. Consequently, the symmetry of the TiO_6 octahedra was slightly improved by Ca substitution, and the TiO_6 octahedra existing in the $(Sr_{0.9}Ca_{0.1})_3(Ti_{0.95}Nb_{0.05})_2O_7$ compound were the most symmetrical among the present compounds.

Figure 2 shows the temperature dependence of σ, μ_{Hall}, and n_c for $(Sr_{1-x}Ca_x)_3(Ti_{1-y}Nb_y)_2O_7$ (x=0, 0.1, y =0.05–0.2). Above 600 K, σ shows the temperature dependence of a degenerate semiconductor, while n_c is constant with temperature for all compositions, and the σ values increase systematically with Nb content with increasing n_c. The μ_{Hall} values depend only slightly on temperature at low temperatures, whereas, reaching higher temperatures (~750 K), a strong temperature dependence in the form of a power law, $\mu_{Hall} \propto T^{-1.5}$, is observed. From the results of similar power-law dependences $\mu_{Hall} \propto T^{-1.5}$ in perovskite-

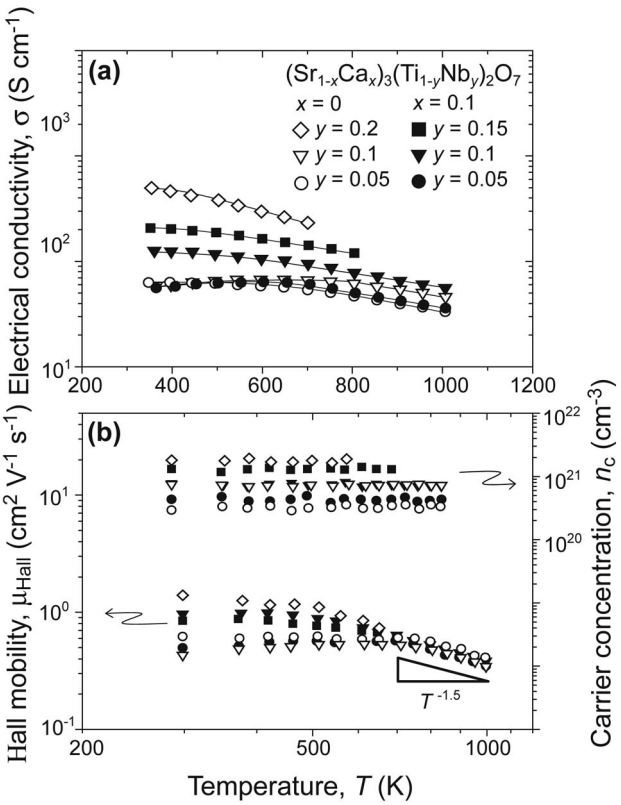

FIG. 2. Temperature dependence of (a) electrical conductivity and (b) Hall mobility and carrier concentration for $(Sr_{1-x}Ca_x)_3(Ti_{1-y}Nb_y)_2O_7$ ($x=0$, 0.1, $y=0.05-0.2$).

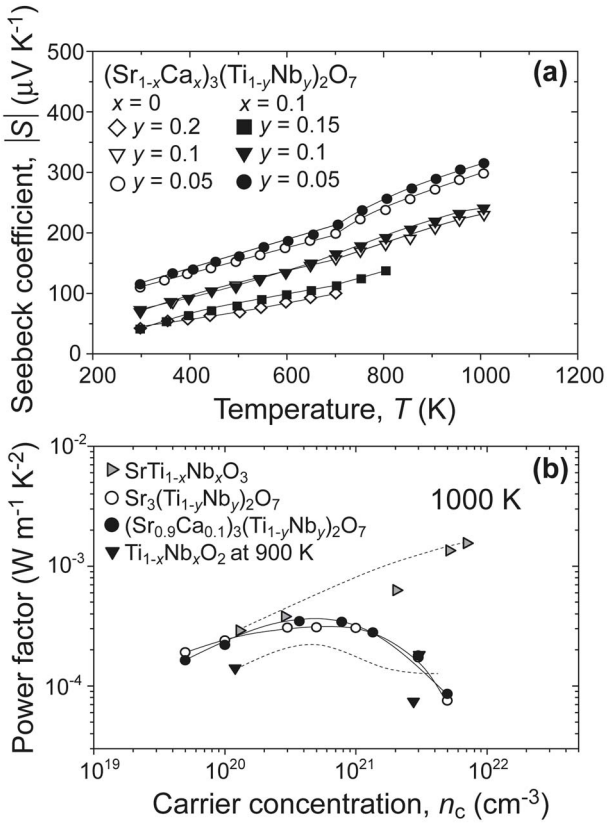

FIG. 3. (a) Temperature dependence of Seebeck coefficient and (b) estimated power factor with carrier concentration for $(Sr_{1-x}Ca_x)_3(Ti_{1-y}Nb_y)_2O_7$ ($x=0$, 0.1, $y=0.05-0.2$). Data for Nb-doped $SrTiO_3$ and TiO_2 epitaxial films are taken from Refs. 11 and 20, respectively.

type $SrTiO_3$ systems, which have indicated that the acoustic phonon scattering mechanism is predominant,[11,16,17] it has been considered that the electrical conduction in RP phases should take place dominantly within the perovskite layers.

Figure 3 shows the temperature dependence of the absolute values of S and the n_c dependence of the power factor (PF) for $(Sr_{1-x}Ca_x)_3(Ti_{1-y}Nb_y)_2O_7$ ($x=0$, 0.1, $y=0.05-0.2$). All samples have negative S, with a gradual increase in magnitude with temperature, indicating that the samples are n-type degenerate semiconductors; the $|S|$ values shows the following behavior: (1) decrease with Nb doping and (2) increase by Ca substitution, especially for 5 at % Nb-doped $Sr_3Ti_2O_7$. Because m^* is one of the main factors determining S, we have calculated the m^* values and examined the transport and structural parameters affecting m^* in order to clarify the variation of S mentioned above. Figure 4 shows m^* as a function of Ti-Ti distance and n_c at 1000 K. Values for the cubic perovskite-type La- and Nb-doped $SrTiO_3$ single crystals[18] and epitaxial films[11,19] and Nb-doped anatase TiO_2 epitaxial films[20] are shown for comparison. The values for $Sr_3(Ti_{0.8}Nb_{0.2})_2O_7$ and $(Sr_{0.9}Ca_{0.1})_3(Ti_{0.85}Nb_{0.15})_2O_7$ were estimated from the measured transport parameters (S and n_c) in high vacuum; details of the calculation of m^* are described elsewhere.[21] The m^* values of the RP phases are not greatly changed with Nb doping, and thus the decrease in S with Nb doping is due to the increase in n_c. On the other hand, μ_{Hall} for La- and Nb-doped $SrTiO_3$ decreases gradually with Ti-Ti distance due to the gradual increase in m^*, while the RP phases show nearly constant values, regardless of Ti-Ti distance, due to the slight change in m^*, as shown in Fig. 4(c).

In many TE materials, the variation behavior of m^* can be explained according to the Kane model,[22] which represents an increase in m^* with increasing charge carrier concentration. However, the m^* values for Ti-based metal oxides appear to be independent of n_c, as shown in Fig. 4(b). In our previous studies on cubic perovskite-type La- and Nb-doped $SrTiO_3$ systems,[11,18] we proposed the Ti-Ti distance as the parameter responsible for determining m^*, and it was found that the increase in m^* by Nb doping did not originate from an increase in n_c but from an increase in the distance between two neighboring Ti ions, which leads to a decrease in the overlap between Ti $3d-t_{2g}$ orbitals. Increases in S by lattice expansion (enlargement of Ti-Ti distance) are observed in other cubic perovskite-type Ba-substituted or Y-doped $SrTiO_3$ systems,[17,23] but this phenomenon is not effective in RP phases with distorted TiO_6 octahedra. Very recently, we have investigated the TE properties of heavily Nb-doped anatase TiO_2 epitaxial films, which also contain distorted TiO_6 octahedra. The carrier generation mechanism and transport properties were basically similar to those of Nb-doped $SrTiO_3$, whereas m^* was an order of magnitude smaller than that of Nb-doped $SrTiO_3$, owing to the crystal field splitting of Ti $3d-t_{2g}$ orbitals, and the PF was much lower than that of cubic perovskite-type Nb-doped $SrTiO_3$, especially at high n_c, as shown in Fig. 3(b). These results indicate that the degraded S of RP phases and Nb-doped

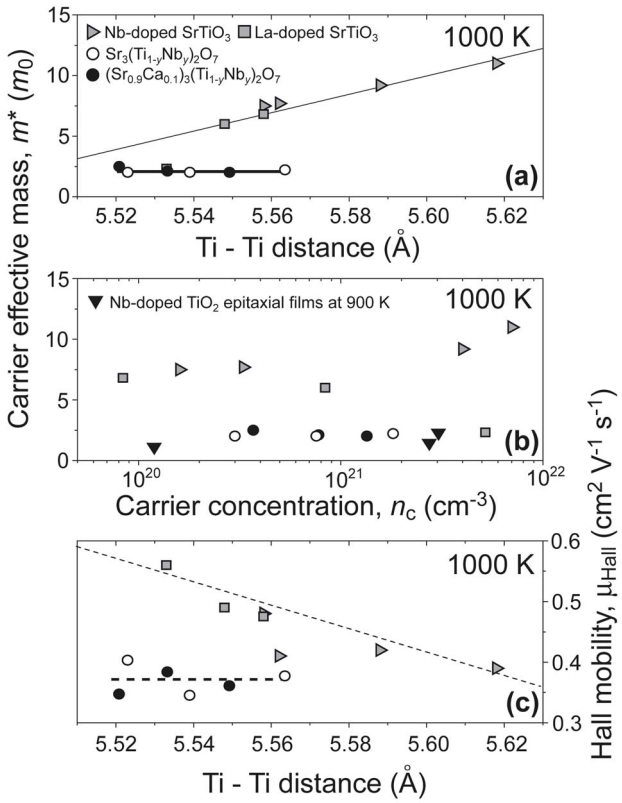

FIG. 4. Carrier effective mass as functions of (a) Ti-Ti distance along [110] and (b) carrier concentration at 1000 K and (c) Hall mobility with Ti-Ti distance. Data for La- and Nb-doped $SrTiO_3$ (at 1000 K) and Nb-doped TiO_2 (at 900 K) epitaxial films are taken from Refs. 19 and 20, respectively.

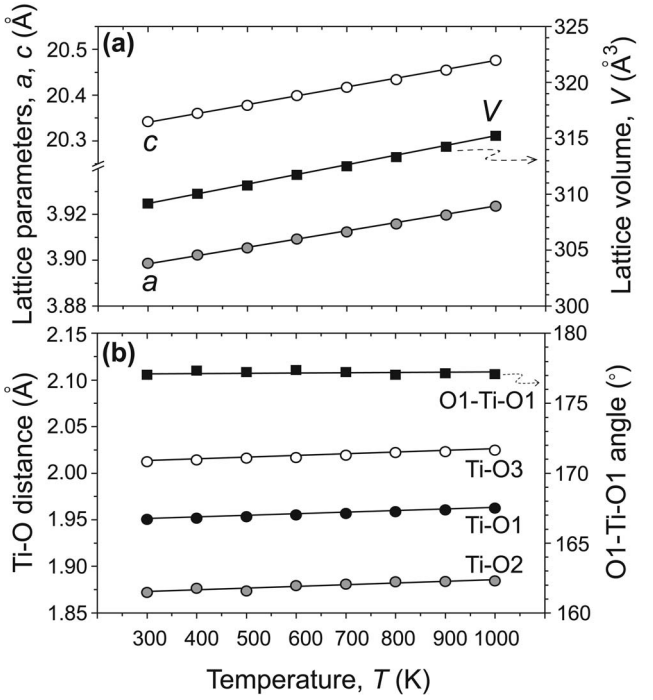

FIG. 5. Temperature dependence of crystallographic parameters for $Sr_3Ti_2O_7$ (a) lattice parameters and volume and (b) Ti-O bond distance and O1-Ti-O1 bond angle.

anatase TiO_2 epitaxial films can be ascribed mainly to the distorted structure of the TiO_6 octahedra. Thus, in order to achieve a high TE performance in Ti-based metal oxides, it is highly desirable that both high symmetry for the TiO_6 octahedra and large length for the Ti-Ti bonds, as in $SrTiO_3$ perovskites, should be maintained.

In spite of the lower n_c values of RP phases compared to those of $SrTiO_3$ phases with the same amount of Nb doping, the S values of the former are lower than those for the latter over the whole temperature range. This result is also explainable from the viewpoint of the crystallographic features, i.e., the distorted TiO_6 octahedra are maintained even at high temperature. Rietveld refinement for $Sr_3Ti_2O_7$ in the temperature range 300 – 1000 K was conducted, and the calculated crystallographic parameters as a function of temperature are summarized in Fig. 5 and Table I. All crystallographic parameters showed a monotonic increase with temperature, except that the angle of the O1-Ti-O1 bond was nearly constant over the whole temperature range, implying that the distorted structure of the TiO_6 octahedra is maintained from room temperature to 1000 K.

By Ca substitution in the RP phases, a slight increase in S was observed in all compounds. From the results that the TiO_6 octahedra become more symmetric by Ca substitution and the symmetry of the TiO_6 octahedra is maintained up to 1000 K, the increase in S by Ca substitution and the variation behavior in m^* of RP phases in Fig. 4 are considered to be caused by the symmetry of the TiO_6 octahedra. This implies that the m^* value can be increased even in compounds containing distorted TiO_6 octahedra by enhancement of the symmetry. The present findings may provide highly useful information for the realization of high TE performance in Ti-based metal oxides. Further investigation is required, especially in RP compounds with larger Ti-Ti distances, as in $SrTiO_3$ perovskites, and thus, Zr^{4+}- (r=72 p.m., coordination number =6, M_{Zr}=91) and Hf^{4+}- (r=71 p.m., coordination number =6, M_{Hf}=178) substituted compositions are under investigation.

Figure 6 shows the temperature dependence of κ for $(Sr_{1-x}Ca_x)_3(Ti_{1-y}Nb_y)_2O_7$ (x=0, 0.1, y=0.05, 0.1). The total thermal conductivity (κ_{tot}) can be expressed by the sum of κ_{lat} and the electronic contribution (κ_{ele}). In our case, κ_{ele} increases with increasing Nb content and by Ca substitution, owing to the increase in n_c. However, the κ_{ele} values estimated by use of the Wiedemann-Franz law are very small ($\kappa_{ele} \sim 0.3$ W m^{-1} K^{-1}) compared to κ_{tot}, which indicates that the phonon contribution is predominant. In addition to the κ reduction by phonon scattering at $SrO/(SrTiO_3)_2$ interfaces

TABLE I. Crystallographic data for $Sr_3Ti_2O_7$ at different temperatures.

T (K)	a (Å)	c (Å)	V (Å^3)	Ti-O1 (Å)	Ti-O2 (Å)	Ti-O3 (Å)	O1-Ti-O1 (°)
300	3.8985(9)	20.3414(4)	309.15	1.9503	1.8720	2.0123	177.03
400	3.9022(3)	20.3600(2)	310.03	1.9516	1.8762	2.0140	177.34
500	3.9052(4)	20.3775(7)	310.78	1.9532	1.8734	2.0160	177.22
600	3.9091(1)	20.3985(9)	311.71	1.9551	1.8792	2.0166	177.37
700	3.9122(3)	20.4166(1)	312.49	1.9567	1.8807	2.0191	177.23
800	3.9157(2)	20.4338(6)	313.31	1.9585	1.8834	2.0221	177.03
900	3.9195(8)	20.4544(2)	314.24	1.9604	1.8838	2.0231	177.15
1000	3.9234(8)	20.4756(1)	315.20	1.9624	1.8844	2.0247	177.08

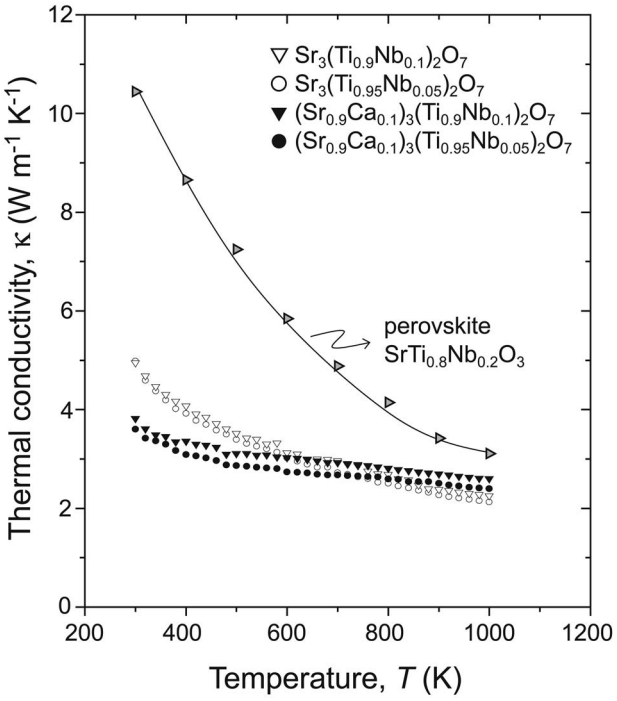

FIG. 6. Temperature dependence of thermal conductivity for 5 and 10 at % Nb-doped $(Sr_{1-x}Ca_x)_3Ti_2O_7$ (x=0, 0.1). The thermal conductivity data for cubic perovskite-type 20 at % Nb-doped $SrTiO_3$ polycrystalline ceramics are taken from the data in Ref. 12.

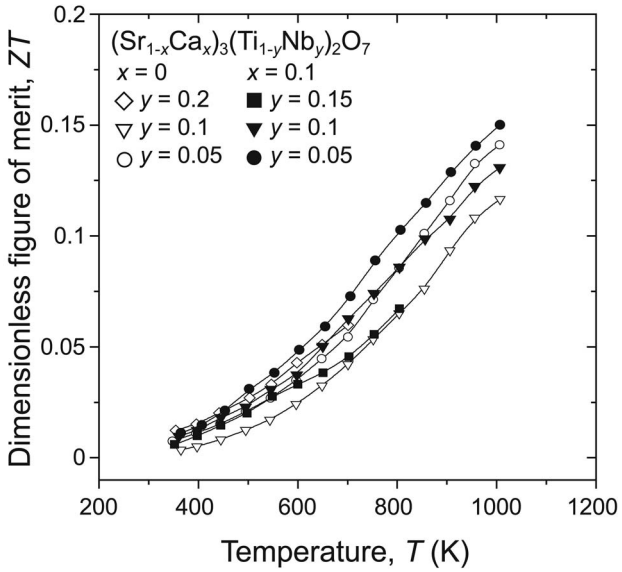

FIG. 7. Temperature dependence of dimensionless thermoelectric figures of merit for $(Sr_{1-x}Ca_x)_3(Ti_{1-y}Nb_y)_2O_7$ (x=0, 0.1, y=0.05–0.2).

originating from the superlattice structure observed in nonsubstituted compositions, additional reduction by Ca substitution was found due to mass-defect phonon scattering between Ca (M_{Ca}=40) and Sr (M_{Sr}=88) at low temperatures, whereas the κ values for Ca-substituted compositions show weak temperature dependence, and κ values were higher than those of nonsubstituted ones above 700 K. From σ, S, and κ values, we have calculated the ZT values for $(Sr_{1-x}Ca_x)_3(Ti_{1-y}Nb_y)_2O_7$ (x=0, 0.1, y=0.05–0.2) and present them in Fig. 7. For all samples, the ZT value increases with temperature over the whole temperature range. Although κ increased slightly at high temperatures by Ca substitution, ZT increased owing to the increase in S and σ, and the largest ZT value (0.15 at 1000 K) was observed for 10 at % Ca-substituted $Sr_3(Ti_{0.95}Nb_{0.05})_2O_7$.

IV. SUMMARY

We investigated the relationship between the transport parameters and the crystallographic parameters for layered perovskite-type $(Sr_{1-x}Ca_x)_3(Ti_{1-y}Nb_y)_2O_7$ (x=0, 0.1, y=0.05–0.2) polycrystalline RP phases. It was found that large S values could be obtained by enhancement of the symmetry of the TiO_6 octahedra resulting in increases in m^*, suggesting the both high TiO_6 symmetry and adequate Ti-Ti distance are required for high TE performance Ti-based metal oxides. In addition to the thermal conductivity reduction by phonon scattering at $SrO/(SrTiO_3)_2$ interfaces of the inherent superlattice structure, there was additional reduction achieved due to the mass-defect phonon scattering between Ca (M_{Ca}=40) and Sr (M_{Sr}=88) at low temperatures. The ZT values increased owing to the increase in S, and the largest ZT value observed (0.15 at 1000 K) was obtained for 10 at % Ca-substituted $Sr_3(Ti_{0.95}Nb_{0.05})_2O_7$.

ACKNOWLEDGMENTS

The authors express their thanks to Dr. Katsuhiko Inaba and Dr. Ryuji Matsuo of Rigaku Corporation and Dr. Kouta Iwasaki of Nagoya University for technical assistance and useful discussions on the high-temperature Rietveld refinement. They also would like to thank Dr. Hideki Kita and Dr. Hideki Hyuga of the National Institute of Advanced Industrial Science and Technology (AIST) and Mr. Akihiro Ishizaki of Nagoya University for sample preparation.

[1] S. N. Ruddlesden and P. Popper, Acta Crystallogr. **10**, 538 (1957).
[2] S. N. Ruddlesden and P. Popper, Acta Crystallogr. **11**, 54 (1958).
[3] S. Miyazawa and M. Mukaida, Appl. Phys. Lett. **64**, 2160 (1994).
[4] J. H. Haeni, C. D. Theis, D. G. Schlom, W. Tian, X. Q. Pan, H. Chang, I. Takeuchi, and X. D. Xiang, Appl. Phys. Lett. **78**, 3292 (2001).
[5] T. Kimura, Y. Tomioka, H. Kuwahara, A. Asamitsu, M. Tamura, and Y. Tokura, Science **274**, 1698 (1996).
[6] Y. S. Zhen and J. B. Goodenough, Mater. Res. Bull. **25**, 785 (1990).
[7] V. V. Kharton, A. P. Viskup, A. V. Kovalevsky, E. N. Naumovich, and F. M. B. Marques, Solid State Ionics **143**, 337 (2001).
[8] X. Yang, L. Luo, and H. Zhong, Appl. Catal. Gen. **272**, 299 (2004).
[9] K. Koumoto, S. Ohta, and H. Ohta, in *Proceedings of the 23rd International Conference on Thermoelectrics* (IEEE, Piscataway, 2005), Vol. 92.
[10] K. H. Lee, S. W. Kim, H. Ohta, and K. Koumoto, J. Appl. Phys. **100**, 063717 (2006).
[11] S. Ohta, T. Nomura, H. Ohta, M. Hirano, H. Hosono, and K. Koumoto, Appl. Phys. Lett. **87**, 092108 (2005).
[12] S. Ohta, H. Ohta, and K. Koumoto, J. Ceram. Soc. Jpn. **114**, 102 (2006).
[13] F. Izumi and T. Ikeda, Mater. Sci. Forum **321**, 198 (2000).
[14] V. M. Goldschmidt, Akad. Oslo I, Mat.-, Nature **2**, 7 (1926).
[15] R. D. Shannon, Acta Crystallogr., Sect. A: Cryst. Phys., Diffr., Theor. Gen. Crystallogr.. **A32**, 751 (1976).
[16] R. Moos and K. H. Härdtl, J. Appl. Phys. **80**, 393 (1996).

[17]H. Muta, K. Kurosaki, and S. Yamanaka, J. Alloy. Compd. **368**, 22 (2004).
[18]S. Ohta, T. Nomura, H. Ohta, and K. Koumoto, J. Appl. Phys. **97**, 034106 (2005).
[19]S. Ohta, Ph.D. thesis, Nagoya University, 2006.
[20]D. Kurita, S. Ohta, K. Sugiura, H. Ohta, and K. Koumoto, J. Appl. Phys. **100**, 096105 (2006).
[21]V. I. Fistul, *Heavily Doped Semiconductors* (Plenum Press, London, 1969).
[22]E. O. Kane, J. Phys. Chem. Solids **1**, 249 (1957).
[23]S. Hui and A. Petric, J. Electrochem. Soc. **149**, J1 (2002).